Invited Paper

Experimental observation of environment-induced sudden death of entanglement

M. P. Almeida*, F. de Melo†, M.O. Hor-Meyll, A. Salles, S.P. Walborn, P.H.Souto Ribeiro, and L. Davidovich

Instituto de Física, Universidade Federal do Rio de Janeiro, Cx. P. 68528
21941-972 Rio de Janeiro, RJ, Brazil

ABSTRACT

We demonstrate, using an all-optical setup, the difference between local and global dynamics of entangled quantum systems coupled to independent environments. Even when the environment-induced decay of each system is asymptotic, quantum entanglement may suddenly disappear.

Keywords: Entanglement, decoherence, twin photons

1. INTRODUCTION

Entanglement and decoherence are closely connected concepts. Their subtleties were brought to light by remarkable papers in the year 1935: that of Einstein, Podolski, and Rosen,[1] which became known as the "EPR paper," and a series of papers by Schrödinger,[2] which contained seminal ideas for the characterization of entanglement, and discussed the famous "cat paradox." The two concepts also play an intertwining and subtle role in quantum-measurement theory.[3,4] It is now clear that the emergence of the classical world from the underlying quantum substrate is intimately connected to the phenomenon of decoherence, which stems from the unavoidable interaction between the system of interest and its environment. A coherent superposition between two states of the system gets entangled with two states of the environment, thus turning the initial state of the system into a mixture.[5,6] The dynamics of decoherence, of crucial importance for the understanding of the quantum-classical boundary, has been the subject of theoretical[7–9] and experimental[10] investigation.

In recent years, entanglement has turned from an intriguing and essential component of quantum physics into a practical tool for communications and computation. In fact, the real-world success of quantum computation[11,12] and communication[13–19] relies on the longevity of entanglement in multi-particle quantum states. The presence of decoherence in communication channels and computing devices degrades the entanglement when the particles propagate or the computation evolves.

Decoherence leads to both local dynamics, associated with single-particle dissipation, diffusion, and decay, and to global dynamics, which may provoke the disappearance of entanglement at a finite time.[20–24] This phenomenon, known as "entanglement sudden death",[24] is strikingly different from single-particle decay, which occurs asymptotically. It has been studied recently by many authors, within the realm of simple models, dealing with a particle in a diffusive bath, or a two-level atom spontaneously emitting radiation.[20–24]

We have demonstrated this effect experimentally, using an all-optical setup, for a two-qubit system interacting with independent environments. In the next Section, we discuss the relevant dynamics of the system considered by us. In Sect. 3 we present the experimental setup. The experimental results are discussed in Sect. 4. Finally, we summarize our conclusions in Sect. 5.

*Present address: Department of Physics, University of Queensland, Brisbane, QLD, 4072, Australia.
†Present address: Max-Planck-Institute for Physics of Complex Systems, Nöthnitzer Str. 38 D-01187 Dresden, Germany.

Noise and Fluctuations in Photonics, Quantum Optics, and Communications
edited by Leon Cohen, Proc. of SPIE Vol. 6603, 660318, (2007)
0277-786X/07/$18 · doi: 10.1117/12.724472

2. THE AMPLITUDE CHANNEL

Consider a two-level quantum system S (upper and lower states $|e\rangle$ and $|g\rangle$, respectively) under the action of a zero-temperature reservoir R. At zero temperature, the reservoir R is in the $|0\rangle_R$ (vacuum) state, and the $S-R$ interaction can be represented by a quantum map, known as the amplitude decay channel:[11]

$$\begin{aligned} |g\rangle_S \otimes |0\rangle_R &\to |g\rangle_S \otimes |0\rangle_R \\ |e\rangle_S \otimes |0\rangle_R &\to \sqrt{1-p}\,|e\rangle_S \otimes |0\rangle_R + \sqrt{p}\,|g\rangle_S \otimes |1\rangle_R \,. \end{aligned} \tag{1}$$

Under this map, the lower state $|g\rangle$ is not affected, while the upper state $|e\rangle$ either decays to $|g\rangle$ with probability p, creating one excitation in the environment (state $|1\rangle_R$), or remains in $|e\rangle$, with probability $1-p$. This would be the situation, for instance, in the spontaneous emission of a two-level atom. In this case, the state $|1\rangle_R$ would correspond to one photon in the reservoir. Under the Markovian approximation, $p = 1 - \exp(-\Gamma t)$, and the decay probability approaches unity exponentially in time. As an initial pure state $a|e\rangle + b|g\rangle$ decays, it gets entangled with the environment, gradually losing its coherence and its purity over time. Complete decay occurs asymptotically in time ($p \to 1$ when $t \to \infty$), when the two-level system is again described by the pure state $|g\rangle$.

One should note that map (1) encompasses several other kinds of dynamics, not necessarily related to decay under the influence of a reservoir, which differ only by the time dependence of the parameter p. Thus, for instance, with $p = \sin^2(gt/2)$, the above map describes the reversible interaction, with Rabi frequency g, between a two-level atom and a high-Q cavity mode. The full Rabi cycle is implemented when p goes from 0 to 1 and then back to 0.

Now consider two entangled qubits that evolve according to map (1). What is then the dynamics of the entanglement of the two-qubit system? Does it mimic the behavior of each qubit, disappearing only when p becomes equal 1 (this corresponds to asymptotic decay, for the reservoir situation, or to half a Rabi cycle, for the reversible case), or does it disappear for some other value of p? In other words, what is the relation between the global entanglement dynamics and the local decay of the constituent subsystems?

2.1. Entanglement and separability

A two-qubit pure state is entangled, or non-separable, if and only if the total state cannot be expressed as a product of the individual qubit states: $|\psi\rangle \neq |\phi\rangle_1 \otimes |\varphi\rangle_2$. Likewise, a mixed bipartite state represented by a density matrix $\hat{\rho}$ is separable if and only if it can be written as a convex sum of products of individual density matrices: $\hat{\rho} = \sum_i p_i \hat{\rho}_i^{(1)} \otimes \hat{\rho}_i^{(2)}$, with $0 \leq p_i \leq 1$. For pure bipartite states, the Von Neumman entropy of each subsystem, defined in terms of the respective partial density matrix, is a measure of entanglement:[25] it is zero for a separable state, and maximal for a maximally entangled state, which corresponds to maximal ignorance about the state of each subsystem. For a mixed state expressed in terms of pure states by $\hat{\rho} = \sum_i p_i |\psi_i\rangle\langle\psi_i|$, one cannot say however that the corresponding measure of entanglement is given by the weighted average of the measures for each of the pure states in this sum, since this decomposition is not unique. One defines then the *entanglement of formation*[26] as the minimum value, over all possible decompositions, of the weighted averages.

2.2. Concurrence

For a two-qubit state $\hat{\rho}$, Wootters[26] introduced as a measure of entanglement the *concurrence* C, given by

$$C = \max\{0, \Lambda\}\,, \tag{2}$$

where

$$\Lambda = \sqrt{\lambda_1} - \sqrt{\lambda_2} - \sqrt{\lambda_3} - \sqrt{\lambda_4}\,, \tag{3}$$

and the quantities λ_i are the positive eigenvalues, in decreasing order, of the matrix

$$\hat{\rho}\,(\sigma_y \otimes \sigma_y)\,\hat{\rho}^*\,(\sigma_y \otimes \sigma_y)\ . \tag{4}$$

Here σ_y is the second Pauli matrix and the conjugation occurs in the computational basis $\{|00\rangle, |01\rangle, |10\rangle, |11\rangle\}$. C quantifies the amount of quantum correlation that is present in the system, and can assume values between 0 (only classical correlations) and 1 (maximal entanglement).

This measure cannot be given, in the most general case, an operational meaning. This implies that, in order to evaluate the concurrence, one needs to fully reconstruct the state of the system. For pure states, it is possible to associate a projective measurement to concurrence, if two copies of the state are available.[27,28] In some cases, even when the state is not pure, it is also possible to attach a physical meaning to concurrence. This is the situation here, as will be shown in Section 2.3

For the dynamics given by Eq. (1), and an initial state of the form

$$|\Phi\rangle = |\alpha|\,|gg\rangle + |\beta|\exp(i\theta)\,|ee\rangle\ , \tag{5}$$

the qubit reduced density matrix is given by

$$\hat{\rho}\,(p) = \begin{pmatrix} |\alpha|^2 + p^2\,|\beta|^2 & 0 & 0 & (1-p)\,|\alpha\beta|\,e^{-i\theta} \\ 0 & (1-p)\,p\,|\beta|^2 & 0 & 0 \\ 0 & 0 & (1-p)\,p\,|\beta|^2 & 0 \\ (1-p)\,|\alpha\beta|\,e^{i\theta} & 0 & 0 & (1-p)^2\,|\beta|^2 \end{pmatrix}\ , \tag{6}$$

where the rows and columns are indexed according to the sequence (gg, ge, eg, ee). The general structure of this density matrix is easily understood: due to the coupling with the environment, the initial coherence between states $|e\rangle$ and $|g\rangle$ vanishes as $p \to 1$. The states $|eg\rangle$ and $|ge\rangle$, on the other hand, are populated by the decay of the initial state, and also feed the state $|gg\rangle$, but no additional coherence is built by the incoherent decay.

From Eq. (6), the concurrence can be easily derived:

$$C = \max\{0, \Lambda\} \quad \text{with} \quad \Lambda = 2\,(1-p)\,|\beta|\,(|\alpha| - p\,|\beta|)\ . \tag{7}$$

One can see that for $|\beta| < |\alpha|$, entanglement disappears only when the individual qubits have completely decayed ($p = 1$), while for $|\beta| > |\alpha|$, entanglement disappears for $p = |\alpha/\beta| < 1$. This implies, for $p = 1 - \exp(-\Gamma t)$ (decaying system), that entanglement will disappear at a finite time, before complete decay of the two-level system. This phenomenon has been called "entanglement sudden death".[24] Since the concurrence of the initial state ($p = 0$) is $C = 2|\alpha\beta|$, the entanglement dynamics of two states with the same initial concurrence can be quite different: the same value of the initial concurrence may correspond to either $|\alpha| > |\beta|$ or $|\alpha| < |\beta|$.

As mentioned before, map (1) also describes the oscillatory exchange of energy between a two-level atom and a cavity mode. In this case, $p = \sin^2(gt/2)$, and one also gets a "sudden death" phenomenon:[29] if $|\beta| > |\alpha|$, entanglement disappears at a time smaller than the Rabi half cycle, when $\sin^2(gt/2) = |\alpha/\beta|$ for the first time, stays zero for a period of time, and is recovered when again $\sin^2(gt/2) = |\alpha/\beta|$. This behavior repeats itself as the Rabi oscillations go on.

2.3. Entanglement Witness

Entanglement witnesses are non-positive operators that are positive on separable states.[30] An operator $\hat{W}$ is an entanglement witness if $Tr(\hat{W}\hat{\rho}) \geq 0$ for any separable state, and there exist entangled states $\hat{\sigma}$ for which $Tr(\hat{W}\hat{\sigma}) < 0$. These operators offer a simple way to characterize entanglement in some cases. Of course, entanglement witnesses allow one to identify some, but not all, entangled states.

For the dynamics described by Eq. (1), and the initial state (5). it is possible to define a "perfect" time-independent witness,[23] so that $-Tr(\hat{W}\hat{\rho})$ coincides precisely with the concurrence of the mixed state $\hat{\rho}$ that evolves from $|\Psi\,(0)\rangle$. That is, $Tr(\hat{W}\hat{\rho})$ becomes positive only when the state becomes separable.

The entanglement witness in this case is given by

$$\hat{W}_\theta \equiv 1 - 2\,|\Phi\,(\theta)\rangle\,\langle\Phi\,(\theta)|\ , \tag{8}$$

where

$$|\Phi\,(\theta)\rangle = \left[|gg\rangle + e^{i\theta}\,|ee\rangle\right]/\sqrt{2}\,.$$

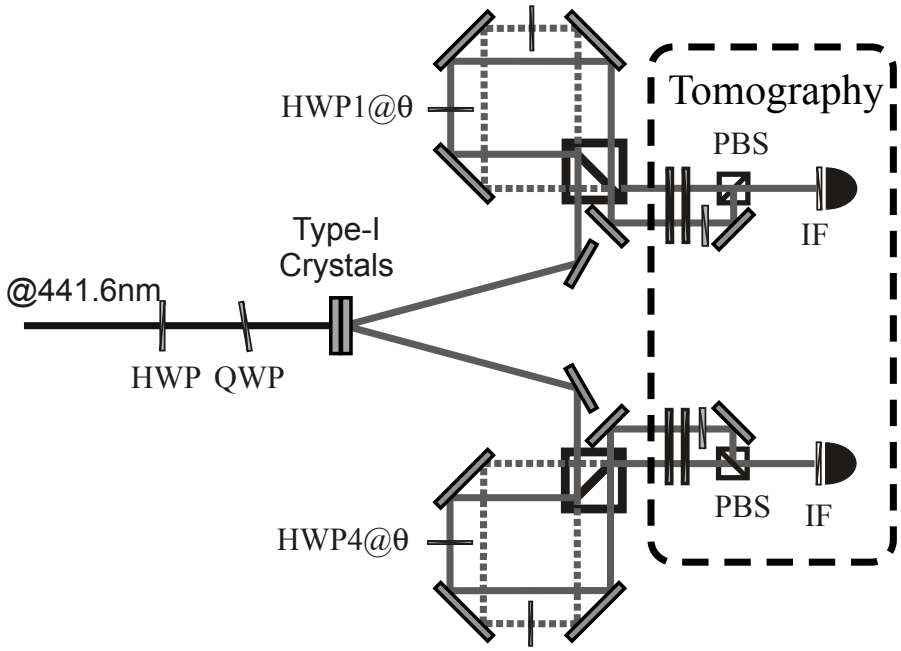

Figure 1. Amplitude-decay channel for an entangled two-photon state, generated by parametric down-conversion in type-I non-linear crystals.

One can then show, from Eqs. (6) and (7), that

$$\Lambda = -Tr\left[\hat{W}_\theta \hat{\rho}\,(t)\right] = 2\left[P\,(\theta, t) - \frac{1}{2}\right],$$

where $P(\theta, t) = Tr[|\Phi(\theta)\rangle\langle\Phi(\theta)|\hat{\rho}(t)]$. This means that the concurrence is equal to twice the excess probability, with respect to 1/2, of finding the state of the system in the maximally entangled state $|\Phi\,(\theta)\rangle$. It is quite remarkable that, in this case, concurrence can be given a simple physical meaning, valid throughout the evolution of the system: it can be determined by measuring the probability of finding the system, initially in the state $|\Phi\rangle$ given by Eq. (5), in the maximally-entangled state $|\Phi\,(\theta)\rangle$.

We show now how map (1) can be implemented with an all-optical setup, based on twin-photon beams.

3. EXPERIMENTAL SETUP

The experimental realization of Eq. (1) is made by associating the H and V polarizations of a photon to the ground and excited states of the two-level system S, respectively. The reservoir R in turn is represented by two different momentum modes of the photon.

The experimental setup is shown in Fig. 1, and may be divided into three blocks: the generation of entangled pairs, the realization of the quantum map, and the quantum-state tomography (QST). These steps are described with detail in the following subsections. We also show how to implement another quantum map, corresponding to a dephasing channel, with a small modification of the setup.

3.1. Entangled-photon source

The polarization-entangled photon pairs are obtained from a two-crystal source[31] composed of two adjacent nonlinear crystals, which are pumped by the same laser, giving rise to parametric down-conversion. The crystals are set with their optic axes perpendicular, so that one of the crystals produces vertically-polarized signal and

idler photons and the other produces horizontally polarized photons. Both crystals produce photons along the same output directions, so that, after propagation and filtering by a pinhole, vertically and horizontally polarized modes become indistinguishable and therefore mutually coherent. The degree of coherence obtained in this process is increased when using thin crystals, large propagation distances, and a narrow pinhole for spatial filtering. This degree of coherence will also determine the degree of purity of the entangled state produced. In our setup, we have used 2mm long $LiIO_3$(lithium Iodate) nonlinear crystals that were pumped with a continuous-wave He-Cd laser oscillating at 442nm. The propagation distances from the crystal to the detector pinholes were about 1,5m for both signal and idler beams and the detection pinhole diameters were about 1mm. Under these conditions, we obtained entangled states with purity of 95% or higher.

The entangled state thus produced is given by:

$$|\psi\rangle = |\alpha||HH\rangle + |\beta|e^{i\theta}|VV\rangle\,, \tag{9}$$

with $|\alpha|^2 + |\beta|^2 = 1$.

The coefficients $|\alpha|$ and $|\beta|$ can be controlled through the polarization of the pump laser. If the pump polarization is linear at $\pi/4$ with respect to the crystal axes, the two crystals will be pumped equally and $|\alpha| = |\beta|$. Other directions of the pump polarization will produce non maximally-entangled states. The phase θ can be controlled by making the pump polarization elliptical, or in other words, introducing a phase difference between horizontal and vertical polarization components. It is also possible to prepare any one of the Bell states, starting from the state given by Eq. (9). Thus, a half-wave plate in one of the beams leads to states like:

$$|\psi\rangle = |\alpha||HV\rangle + |\beta|e^{i\theta}|VH\rangle. \tag{10}$$

3.2. Interaction with the environment

The crucial part of our experiment is realization of map (1). Fig. 2 shows the interferometer that implements the interaction of the photon polarization with the environment as described by map (1). The main idea behind the interferometer is to separate the horizontal (H) and vertical (V) polarization components of a light beam

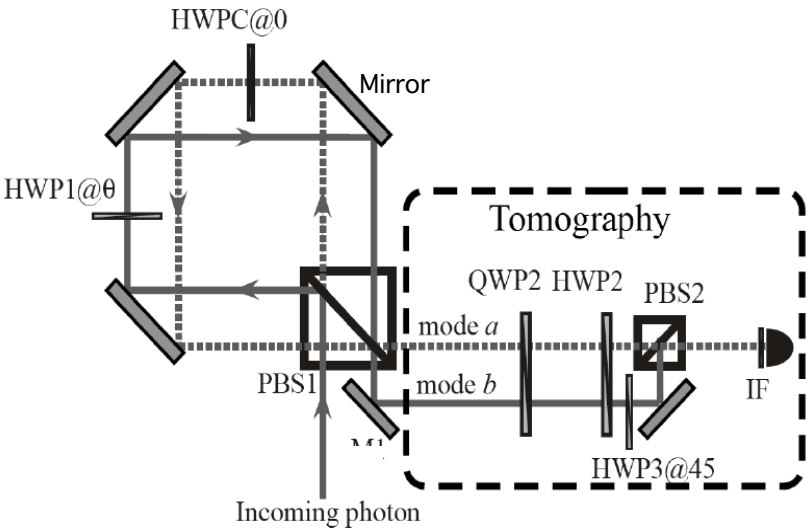

Figure 2. Amplitude-decay channel for a single photon.

and to be able to manipulate each one of these polarization modes independently, recombining them coherently afterwards. This task requires substantial interferometric stability, as this operation is performed on both signal and idler photons, and any interferometric fluctuations will give rise to uncontrolled decoherence of the input entangled state.

Sagnac interferometers are very stable and are thus good candidates for our application. In a polarization-dependent Sagnac interferometer, H- and V-polarization components are separated in a polarized beam-splitter and propagate in opposite directions inside the interferometer, eventually exiting through the same port of the input/output beam-splitter. The remarkable stability comes from the fact that both H- and V-polarization components of the field propagate through the same path, though in opposite directions. Thus they both suffer the same mechanical or thermal fluctuations, which leads to excellent stability. However, this exact configuration is not adequate for our purposes, since it does not allow the independent manipulation of the polarization components.

The interferometer shown in Fig. 2 is a Sagnac-like interferometer modified to allow independent actions on the different polarization modes. The modification consists in aligning the mirrors inside the interferometer in such a way that H- and V-polarization components are not exactly counter-propagating, but rather follow parallel paths. Using this configuration, we were able to achieve high stability and at the same time we could insert the half-wave plate (HWP1) in the V polarization mode and a compensation plate (HWPC) in the H mode. HWP1 will be used in the implementation of a reservoir and HWPC is necessary in order to balance the optical paths, after HWP1 is introduced.

In this modified Sagnac, a photon, initially in the incoming part of mode a, is split into its horizontal (H) and vertical (V) polarization components by a polarizing beam splitter (PBS1). Let us ignore the half-wave plates HWP1 and HWPC for the moment. The V-polarization component is reflected and propagates through the interferometer in the clockwise direction, and, if unaltered, reflects through PBS1 into the outgoing part of mode a. The H-polarization component is transmitted and propagates through the interferometer in the counter-clockwise direction and transmits through PBS1, also into the outgoing part of mode a.

To realize the amplitude decay given in map (1), we use HWP1 to rotate the polarization of the V component to $\cos(2\theta)|V\rangle + \sin(2\theta)|H\rangle$, where θ is the angle of HWP1. Suppose that an incoming photon is V-polarized. When this photon exits the interferometer through PBS1, it is transmitted into mode b with probability $p = \sin^2(2\theta)$ and reflected into mode a with probability $\cos^2(2\theta)$. This evolution can thus be described by $|V\rangle|a\rangle \longrightarrow \sqrt{1-p}|V\rangle|a\rangle + \sqrt{p}|H\rangle|b\rangle$. Identifying the outgoing modes a and b (which correspond to orthogonal spatial modes) as the states of the reservoir with zero and one excitation, respectively, this operation is equivalent to that on the $|e\rangle|0\rangle_R$ state in map (1). An incoming H-polarized photon is left untouched, corresponding to the first line in Eq. (1). This process realizes therefore the amplitude-decay channel, and is identical to the decay of a two-level system. Half-wave plate HWPC, oriented at 0°, is used solely to match the lengths of the two optical paths. The path lengths are adjusted so that if HWP1 is oriented at 0°, the polarization state in mode a after the interferometer is exactly the same as the input state.

3.3. Dephasing reservoir

A simple modification of the present scheme leads to the phase-damping channel, described by the map:[11]

$$\begin{aligned} |g\rangle_S \otimes |0\rangle_R &\rightarrow |g\rangle_S \otimes |0\rangle_R \\ |e\rangle_S \otimes |0\rangle_R &\rightarrow \sqrt{1-p}\,|e\rangle_S \otimes |0\rangle_R + \sqrt{p}\,|e\rangle_S \otimes |1\rangle_R\,. \end{aligned} \tag{11}$$

This map could represent elastic scattering between atom and reservoir. States $|e\rangle$ and $|g\rangle$ are not changed by the interaction, but any coherent superposition of them gets entangled with the reservoir. There is no longer decay, but only loss of coherence between ground and excited states. The dephasing map can be implemented with the same interferometer through the addition of an extra HWP at 45° in mode b before the quantum-state tomography system (or, equivalently, through the removal of HWP3 and redefinition of the QST measurements). For the dephasing channel, all initial states of the form (5) present identical behavior, becoming completely disentangled only when $p = 1$.

3.4. Quantum-state tomography

After the interferometer step, one performs quantum-state tomography of the polarization state of the photon pair, disregarding the environment degrees of freedom (modes a and b). Conceptually, the simplest way of doing this would be to send photons in modes a and b side by side through wave-plates and a polarizer, so that both modes are detected together in the same detector. The problem with this approach is that photon counters do not detect over large areas. The most efficient detectors available are based on avalanche photodiodes, which have small sensitive areas in order to reduce dark counts. We have thus used the scheme shown in Figs. 1 and 2 (tomography block). Modes a and b propagate together through two wave plates, QWP2 and HWP2, shown in Fi. 2. Mode b propagates through an additional half-wave plate HWP3, set at $\pi/4$, so that the horizontal polarization of a photon in this mode is turned into a vertical polarization, which is reflected by the polarized beam splitter PBS2. In this way, modes a and b are recombined at the polarizing beam splitter PBS2. QWP2 and HWP2 implement polarization transformations on both modes, necessary to the polarization tomography. After propagation through QWP2 and HWP2, we must project both modes a and b onto the same linear polarization and detect each of them. This is done by using the two input ports of PBS2, so that the two modes are detected with the same detector. Projection of mode a onto the H polarization is equivalent to projection of mode b onto the V polarization, after it propagates through HWP3. In addition to allowing the coupling and simultaneous analysis of modes a and b, the fact that the optical path from PBS1 to PBS2 is larger for mode b than for mode a assures that modes a and b are orthogonal. The path-length difference (about 5 cm) is much larger than the coherence length of the photons, but small enough to ensure that photon pairs in different combinations of modes a and b (of each interferometer) are detected in the coincidence detection window. Our coincidence window is 5 ns, corresponding to a propagation distance of about 1.5 m, which is much larger than the path length difference (5 cm). Counts were registered with single-photon counting modules (SPCM-AQR14-Perkin Elmer) based on avalanche photodiodes. The detectors are equipped with interference filters with central wavelength around 884nm and bandwidths of 10nm.

Polarization tomography was performed for both single photons and photon pairs. In both cases tomography consists of performing projections onto different polarization states and using the resulting statistics of each projection to reconstruct the density matrix of the single- or two-photon polarization state. These projections were implemented using a quarter-wave plate QWP2, a half-wave plate HWP2 and a linear polarization analyzer PBS2.

For a single qubit, it is implemented by measuring the expectation values of the Pauli operators. When the qubit is encoded in the polarization of a photon, this amounts to determining its Stokes parameters, or, equivalently, to measuring its polarization in any tomographically complete basis consisting of 4 states. The four projections are onto horizontal-, vertical-, diagonal- and circular-polarization states.

For two photons one has to measure the expectation value of all products of two Pauli operators, or, again, measure the photons polarization in any tomographically complete basis, now consisting of 16 two-photon states. We followed a quantum-state tomography procedure,[32] where coincidence counting rates are measured for 16 combinations between four projections in each of the signal and idler beams. The resulting coincidence statistics for the 16 combinations are used to reconstruct the density matrix.

From the coincidence counts in all 16 settings, the density matrix can be reconstructed through a set of linear equations. However, as the raw data have intrinsic statistical errors, the resulting state may turn out to be non-physical. To overcome this problem, we implemented a χ^2 minimization procedure by which the physical (normalized and positive semidefinite) density matrix that best fitted the data was obtained.

The Poissonian uncertainties in the coincidence counts were propagated to uncertainties in the derived quantities (as purity or concurrence) by Monte Carlo simulation as follows.[33] First, we randomly generated counts from a Poissonian distribution with the same mean as the data for each angle setting. We then reconstructed a physical density matrix using the same minimization technique as above. Finally, from this density matrix we computed the value of the derived quantities. A sample for each of these quantities was generated by iterating this process many times (250 in our case), enough to guarantee convergence of its standard deviation, which was in turn used as an estimation of the uncertainty in the desired quantity.

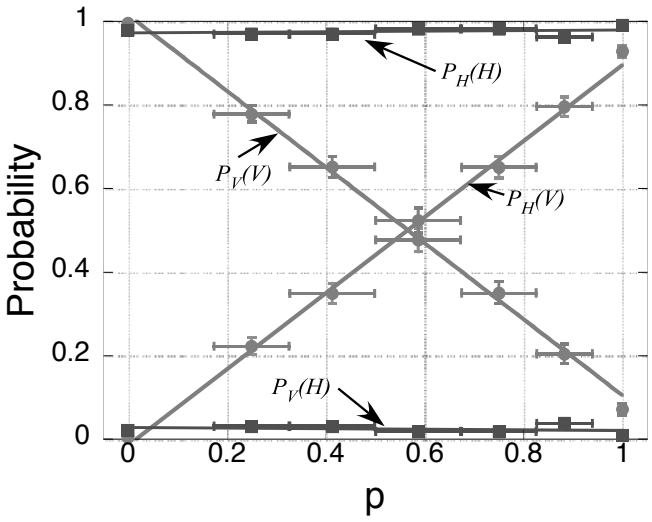

Figure 3. Experimental amplitude decay for a single qubit. $P_V(V)$ and $P_H(V)$ are the probabilities of detecting an input V-polarized photon in the V and H states, respectively. $P_V(H)$ $P_H(H)$ are the the probabilities for an input H photon. The points correspond to experimental data, and the lines are linear fits.

4. EXPERIMENTAL RESULTS

The first step in our experiment was to test the interferometers realizing the amplitude decay channel. This was done by investigating the decay of a single qubit. We have sent both H and V-polarized single photons through the interferometer and perfomed polarization-state tomography. The single photons were obtained from two-photon product states $|VV\rangle$ and $|HH\rangle$. Coincidence counts were registered, with one photon propagating through the interferometer and the other propagating directly to the detector and serving as a trigger, in order to reduce background noise.

Fig. 3 shows $P_V(V)$, $P_H(V)$, $P_V(H)$ $P_H(H)$ as a function of p, where $P_J(K)$ is probability of finding an input K-polarized photon in the J state after the interferometer. The linear behavior in p is associated to an exponential decay in t, if $p = 1 - \exp(-\Gamma t)$ and to Rabi oscillations if $p = \sin^2(gt/2)$.

For the investigation of entanglement dynamics, non-maximally entangled states were produced, and each photon sent to a separate interferometer, which implemented an amplitude-damping reservoir, and then to a QST system. The half-wave plates HWP1 and HWP4 were set to the same angle θ, so that the reservoirs, though independent, acted with the same probability p. QST of the two-photon state followed the usual recipe of 16 coincidence measurements,[32] each lasting 90s, giving an average of about 250 coincidence events. We repeated the same procedure for different values of p, obtaining the tomographic reconstruction of the output two-photon polarization state in all cases.

We have investigated two experimental states that, although not pure, are very close to $|\Phi\rangle = |\alpha||HH\rangle + |\beta|e^{i\delta}|VV\rangle$: state I, defined by $|\beta|^2 = |\alpha|^2/3$, and state II, defined $|\beta|^2 = 3|\alpha|^2$. Tomography of the initial states I and II showed them to have the same concurrence (~ 0.8), and similar purity ($\sim 0.91 - 0.97$). Figs. 4a and 4b show the tomographic reconstructions of the initial ($p = 0$) and final ($p = 1$) states, for the initial states I and II, respectively.

The concurrence was calculated using Eqs. (2) and (3). In all figures, horizontal error bars represent uncertainty in aligning the waveplates, and vertical error bars correspond to the standard deviations of Monte Carlo samples obtained from randomly generated counts following the statistics of the experimental data,[33] as described before.

Figure 5 displays the concurrence and the quantity Λ, given by Eq. 3, as a function of the decay probability p, for the initial states I (triangles) and II (squares). The theoretical curves were obtained by applying map (1) to the

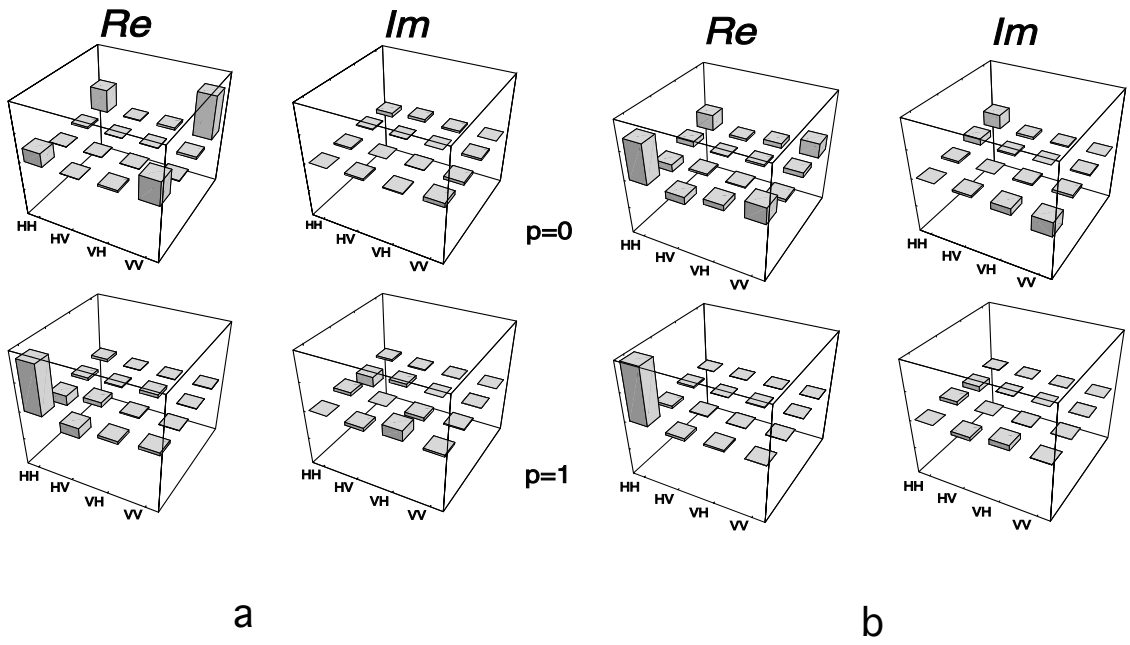

Figure 4. Tomographic reconstructions for the initial ($p = 0$) and final ($p = 1$) entangled states, which are initially very close to $|\Phi\rangle = |\alpha||HH\rangle + |\beta|e^{i\delta}|VV\rangle$: (a) State I, corresponding to $|\beta|^2 = |\alpha|^2/3$; (b) State II, corresponding to $|\beta|^2 = 3|\alpha|^2$.

experimentally-determined initial states, which correspond to $p = 0$. For initial state I, entanglement disappears asymptotically, and the concurrence goes to zero only when both individual systems have decayed completely ($p = 1$). For initial state II, however, the entanglement behaves very differently: the concurrence goes to zero for $p < 1$, thus demonstrating "entanglement sudden death." We stress that the onset of separability ($C = 0$) occurs at the same point for all entanglement quantifiers, and is not a particular artifact of the concurrence.

Figure 6 displays $-Tr(\hat{W}\hat{\rho})$, defined by (8), together with the quantity Λ defined by Eq. (3). As expected, since the initial state is not pure, $-Tr(\hat{W}\hat{\rho})$ does not coincide exactly with the concurrence for entangled states, but it provides a lower bound: it vanishes before the concurrence does, implying that it is not able to identify all entangled states.

It is also illustrative to study the purity, defined as $\mathrm{tr}\hat{\rho}^2$, as a function of the decay probability (Fig. 7) for states I and II. In both cases the purity reaches a minimum but is restored when $p = 1$, when all photons have "decayed" to the H-polarization state. State II is more mixed than state I in the intermediate stages of this process since it has a larger $|VV\rangle$ component, and thus becomes more entangled with the environment.

For the dephasing channel, pure states I and II present identical behavior, becoming completely disentangled only when $p = 1$. Fig. 8 shows the concurrence (squares) and bipartite purity (triangle) as a function of p for the entangled state II.

5. CONCLUSION

We have demonstrated experimentally the phenomenon of sudden disappearance of entanglement for a system of two qubits, interacting with independent environments. For given environments, states with the same initial concurrence may exhibit either an abrupt or an asymptotic disappearance of entanglement, even if the constituents of the system exhibit asymptotic decay. We have explicitly demonstrated that this behavior also depends on the characteristics of the reservoir, through two examples, corresponding to amplitude decay and dephasing.

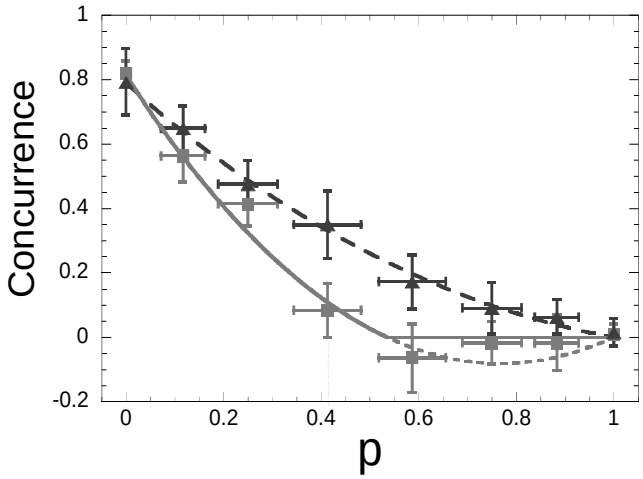

Figure 5. Entanglement decay as a function of the probability p. The squares correspond to experimentally obtained values of Λ for the case $|\beta|^2 = 3|\alpha|^2$. The solid line is the theoretical prediction of the concurrence for this state, given by Eq. 2, while the dotted line shows the value of Λ, given by Eq. 3. The triangles are experimental values of Λ for the case $|\beta|^2 = |\alpha|^2/3$, and the dashed line is the theoretical prediction for Λ and C, which are equivalent for this state.

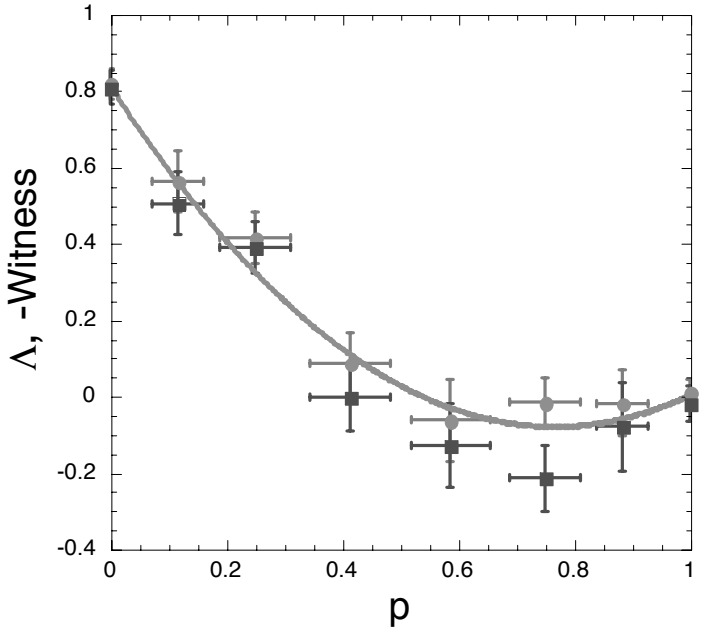

Figure 6. Comparison between Λ, given by Eq. (3), and entanglement witness. The black squares correspond to minus the witness, the gray circles correspond to Λ, determined from the tomographically reconstructed state, for each value of p, and the gray curve is the theoretical prediction for Λ, obtained by applying Eq. (1) to the initial state.

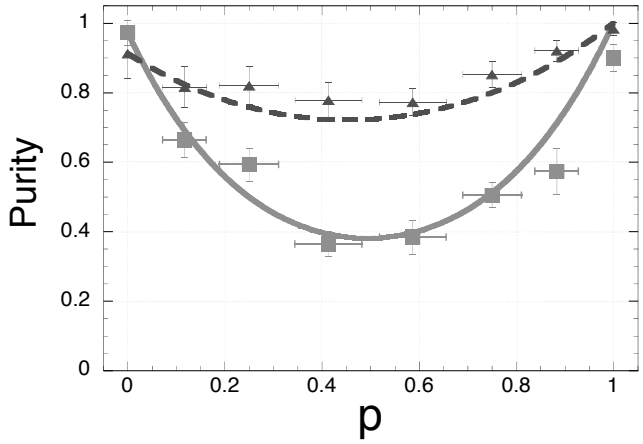

Figure 7. Purity as a function of p for the amplitude-damping channel. The squares correspond to experimentally obtained values of the purity for the case $|\beta|^2 = 3|\alpha|^2$, while the solid line is the theoretical prediction. The triangles are experimental values of the purity for the case $|\beta|^2 = |\alpha|^2/3$, and the dashed line is the corresponding theoretical prediction.

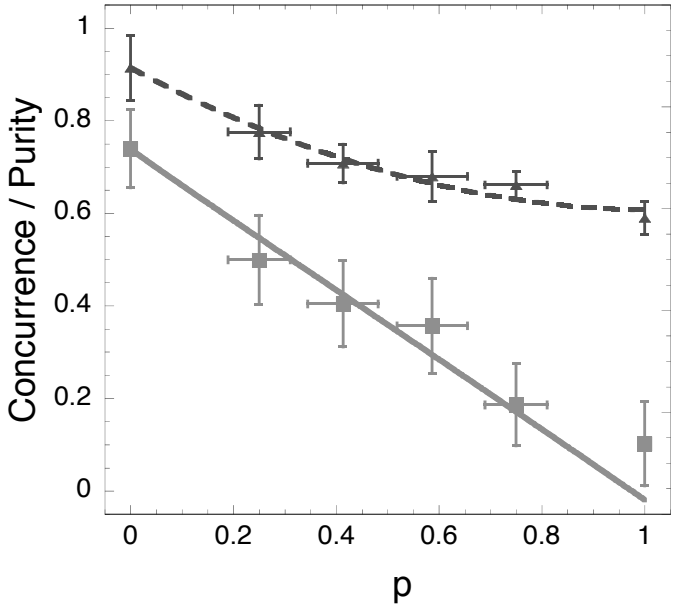

Figure 8. Experimental results for the dephasing channel. Concurrence (squares) and purity (triangles) are shown for the case $|\beta|^2 = 3|\alpha|^2$. The solid line is the corresponding theoretical prediction for concurrence, given by Eq. 2. The dashed line is the theoretical prediction for purity, given by $\mathrm{tr}\hat{\rho}^2$. The concurrence goes to zero asymptotically.

Our approach includes several kinds of dynamics, as for instance Rabi oscillations of a pair of two-level atoms interacting with two independent field modes in a cavity. The experimental setup represents a reliable and simple method for studying the dynamics of entangled systems interacting with controlled environments.

ACKNOWLEDGMENTS

The authors acknowledge financial support from the Brazilian funding agencies CNPq, CAPES, PRONEX, FUJB and FAPERJ. This work was performed as part of the Brazilian Millennium Institute for Quantum Information.

REFERENCES

1. A. Einstein, E. Podolsky, and N. Rosen, "Can quantum-mechanical description of reality be considered complete?," *Phys. Rev. A* **47**, pp. 777–780, 1935.
2. E. Schrödinger, "Die gegenwartige situation in der quantenmechanik," *Naturwissenschaften* **23**, pp. 807–812; 823–828; 844–849, 1935.
3. J. V. Neumann, *Die Mathematische Gundlagen der Quantenmechanik*, Springer-Verlag, Berlin, 1932.
4. J. A. Wheeler and W. H. Zurek, eds., *Quantum Theory and Measurement*, Princeton University Press, Princeton, 1983.
5. W. H. Zurek, "Decoherence, einselection, and the quantum origins of the classical," *Rev. Mod. Phys.* **75**, pp. 715–775, 2003.
6. L. Davidovich, "Decoherence, quantum information, and quantum-state measurement in quantum optics," in *Theoretical and Computational Nanotechnology*, M. Rieth and W. Schommers, eds., **7**, pp. 329–394, American Scientific Publishers, 2006.
7. R. Omnès, *The Interpretation of Quantum Mechanics*, Princeton University Press, Princeton, 1994.
8. D. Giulini, E. Joos, C. Kiefer, J. Kupsch, I.-O. Stamatescu, and H. Zeh, *Decoherence and the Appearance of a Classical World in Quantum Theory*, Springer-Verlag, Berlin, 1996.
9. L. Davidovich, M. Brune, J. Raimond, and S. Haroche, "Mesoscopic quantum coherences in cavity QED: Preparation and decoherence monitoring schemes," *Phys. Rev. A* **53**, pp. 1295–1309, 1996.
10. M. Brune, E. Hagley, J. Dreyer, X. Maître, C. Wunderlich, J. Raimond, and S. Haroche, "Observing the progressive decoherence of the 'meter' in a quantum measurement," *Phys. Rev. A* **77**, pp. 4887–4891, 1996.
11. M. Nielsen and I. Chuang, *Quantum Computation and Quantum Information*, Cambridge, Cambridge, 2000.
12. C. H. Bennett and D. P. DiVincenzo, "Quantum information and computation," *Nature* **404**, pp. 247–255, 2000.
13. C. H. Bennett and G. Brassard, "Quantum cryptography: Public-key distribution and coin tossing," in *Proceedings of the International Conference on Computer Systems and Signal Processing, Bangalore, India*, p. 175, IEEE, New York, 1984.
14. A. K. Ekert, "Quantum cryptography based on Bell's theorem," *Phys. Rev. Lett.* **67**, pp. 661–664, 1991.
15. N. Gisin, G. Ribordy, W. Tittel, and H. Zbinden, "Quantum cryptography," *Rev. Mod. Phys.* **74**, pp. 145–195, 2002.
16. C. H. Bennett, G. Brassard, C. Crépeau, R. Jozsa, A. Peres, and W. K. Wooters, "Teleporting an unknown quantum state via dual classical and Einstein-Podolsky-Rosen channels," *Phys. Rev. Lett.* **70**, pp. 1895–1899, 1993.
17. D. Bouwmeester, J. Pan, K. Mattle, M. Eibl, H. Weinfurter, and A. Zeilinger, "Experimental quantum teleportation," *Nature* **390**, pp. 575–579, 1997.
18. D. Boschi, S. Branca, F. DeMartini, L. Hardy, and S. Popescu, "Experimental realization of teleporting an unknown pure quantum state via dual classical and Einstein-Podolsky-Rosen channels," *Phys. Rev. Lett.* **80**, pp. 1121–1124, 1998.
19. L.-M. Duan, M. D. Lukin, J. I. Cirac, and P. Zoller, "Long-distance quantum communication with atomic ensembles and linear optics," *Nature* **414**, pp. 413–418, 2001.
20. L. Diósi, "Progressive decoherence and total environment disentanglement," in *Irreversible Quantum Dynamics*, F. Benatti and R. Floreanini, eds., pp. 157–164, Springer, Berlin, 2003.

21. P. J. Dodd and J. J. Halliwell, "Disentanglement and decoherence by open system dynamics," *Phys. Rev. A* **69**, pp. 052105–1 – 052105–4, 2004.
22. T. Yu and J. H. Eberly, "Finite-time disentanglement via spontaneous emission," *Phys. Rev. Lett.* **93**, pp. 140404–1 – 140404–4, 2004.
23. M. F. Santos, P. Milman, L. Davidovich, and N. Zagury, "Direct measurement of finite-time disentanglement induced by a reservoir," *Phys. Rev. A* **73**, pp. R040305–1 – R040305–4, 2006.
24. T. Yu and J. H. Eberly, "Quantum open system theory: Bipartite aspects," *Phys. Rev. Lett.* **97**, pp. 140403–1 – 140403–4, 2006.
25. C. H. Bennett, H. J. Bernstein, S. Popescu, and B. Schumacher, "Concentrating partial entanglement by local operations," *Phys. Rev. A* **53**, pp. 2046–2052, 1996.
26. W. K. Wootters, "Entanglement of formation of an arbitrary state of two qubits," *Phys. Rev. Lett.* **80**, pp. 2245–2248, 1998.
27. S. P. Walborn, P. H. S. Ribeiro, L. Davidovich, F. Mintert, and A. Buchleitner, "Experimental determination of entanglement with a single measurement," *Nature* **440**, pp. 1022–1024, 2006.
28. S. P. Walborn, P. H. S. Ribeiro, L. Davidovich, F. Mintert, and A. Buchleitner, "Experimental determination of entanglement by a projective measurement," *Phys. Rev. A* **75**, pp. 032338–1 – 032338–9, 2007.
29. M. Yönac, T. Yu, and J. Eberly, "Sudden death of entanglement of two Jaynes-Cummings atoms," *J. Phys. B: At. Mol. Opt. Phys.* **39**, pp. S621–S625, 2006.
30. R. F. Werner, "Quantum states with Einstein-Podolsky-Rosen correlations admitting a hidden-variable model," *Phys. Rev. A* **40**, pp. 4277–4281, 1989.
31. P. G. Kwiat, E. Waks, A. G. White, I. Appelbaum, and P. H. Eberhard, "Ultrabright source of polarization-entangled photons," *Phys. Rev. A.* **60**, pp. R773–R776, 1999.
32. D. F. V. James, P. G. Kwiat, W. J. Munro, and A. G. White, "Measurement of qubits," *Phys. Rev. A* **64**, pp. 052312–1 – 052312–15, 2001.
33. J. B. Altepeter, E. R. Jeffrey, and P. G. Kwiat, "Photonic state tomography," in *Advances in Atomic, Molecular and Optical Physics*, P. Berman and C. Lin, eds., **52**, p. 107, Elsevier, 2005.